



Analysis of aerodynamic effects and load spectrum characteristics in high-speed railway tunnels

Feilong Li^{a,b}, Jianjun Luo^{a,b,*}, Lei Wang^{a,b}, Dilong Guo^c, Liping Gao^{a,b}

^a Key Laboratory of Urban Underground Engineering of the Ministry of Education, Beijing Jiaotong University, Beijing, 100044, China

^b Beijing's Key Laboratory of Structural Wind Engineering and Urban Wind Environment, Beijing Jiaotong University, Beijing, 100044, China

^c Key Laboratory of Mechanics in Fluid Solid Coupling System, Institute of Mechanics, Chinese Academy of Sciences, Beijing, 100190, China

ARTICLE INFO

Keywords:

High-speed train
Tunnel wall
Peak pressure
Pressure gradient

ABSTRACT

To study the aerodynamic effects and load spectra caused by high-speed trains passing through double-track tunnels, this paper uses unsteady, viscous, compressible Navier-Stokes equations and the Re-Normalization Group $k-\epsilon$ turbulence model with sliding grid technology for simulation. A dynamic model test is carried out to verify the calculation method and grid. This study considers the impact of the three main factors of the tunnel aerodynamic effect when the train passes through the tunnel. The peak of the aerodynamic load spectrum when the train is coupled to the tunnel is mainly concentrated in the range of 0–5 Hz. The results show that as the train speed increases, the peak pressure and pressure gradient increase significantly, and the maximum pressure gradient appears in the time between the peak and trough of the head wave. When two trains meet in the middle of the tunnel, the peak pressure and its position change significantly, and the maximum pressure gradient peaks reach 80.58 kPa/s. When two trains exit the tunnel, the pressure presents a fixed period of fluctuations, and the maximum pressure peak is only 0.09 kPa less than the peak when a single train passes through the tunnel at the same monitoring point.

1. Introduction

In an actual train test of Beijing-Shanghai high-speed rail, the top speed reached 486.1 km/h (Zhao et al., 2012). In 2007, during the trial operation of the improved Train à Grande Vitesse (TGV, the French high-speed railway system) train on the eastern line of the French high-speed railway, the maximum speed reached 575 km/h. As railways continue to reach higher speeds, research on the aerodynamic effects of high-speed railways is particularly important (Zhao et al., 2012). High-speed railways are being constructed in many parts of China, and they will inevitably include cross-mountain areas and incorporate tunnels. By the end of 2019, China had built 3442 high-speed railway tunnels with a total length of 5515 km; the cumulative length of high-speed railway tunnels under construction with a design speed target value of 250–350 km/h is about 2560 km, out of a total of about 7975 km (Tian and Gong, 2020). The length and growth rate of high-speed railway tunnels in China have become the highest in the world (Tian and Gong, 2020), and the number of high-speed railway

tunnels in other countries has also shown an upward trend. When a high-speed train enters a tunnel from an open line, the space around the train will suddenly become smaller, and the gas pressure in front will rise, forming a compression wave at the entrance of the tunnel that propagates to the exit at the speed of sound. When the rear of the train enters the tunnel, the space originally occupied by the car body at the tunnel entrance is suddenly vacated due to its passage. The gas originally squeezed by the car body at the tunnel entrance is released, and the pressure drops suddenly to form an expansion wave, which will travel across the train to the tunnel exit at the speed of sound. At this time, the compression and expansion waves repeatedly circulate in the tunnel. Combined with the train wind in the tunnel, the coupled aerodynamic load is likely to cause fatigue damage to the tunnel and train structures.

Some scholars have studied the durability and mechanical properties of tunnel linings and the strength of train bodies based on aerodynamic loads. Ji (2017) used the fluid mechanics analysis method of tunnel aerodynamics and the structural mechanics analysis method to study the force when there are cavities in different areas behind the secondary

Abbreviations: RNG, Re-Normalization Group; TGV, Train à Grande Vitesse.

* Corresponding author. Key Laboratory of Urban Underground Engineering of the Ministry of Education, Beijing Jiaotong University, No.3 Shangyuncun, Haidian District, Beijing, 100044, China.

E-mail address: jjluo@bjtu.edu.cn (J. Luo).

<https://doi.org/10.1016/j.jweia.2021.104729>

Received 8 March 2021; Received in revised form 20 July 2021; Accepted 20 July 2021

Available online 27 July 2021

0167-6105/© 2021 Elsevier Ltd. All rights reserved.

lining of the vault. It is concluded that the change law of the transient stress generated on the lining structure is consistent with the change law of the aerodynamic load. When the train speed is 350 km/h, the maximum transient stress on the secondary lining structure is about 39 times the aerodynamic load at the same time. [Ma et al. \(2011\)](#) selected the lining concrete within 6° of the lining vault of the tunnel section as the research object. A meso-mechanical model of concrete with initial pores was established to simulate the mechanical properties of the concrete of the tunnel's mid-section lining and vault under high-speed train operation. It is found that the fatigue damage of the tunnel lining concrete structure under repeated compression-tension loads affects the durability of the tunnel lining concrete. Based on the fact that when a high-speed train passes through a tunnel, the air pushed by the running car body is constrained by the tunnel wall to form a strong impact airflow. [Yang and Cui \(2020\)](#) analyzed the process of damage caused by aerodynamic effects in high-speed rail tunnels to facilities at special locations and the characteristics of the formation of traces, which can provide a theoretical basis for accurately determining the nature of the incident and the cause of the accident. [Lu et al. \(2014\)](#) evaluated the fatigue strength of high-speed train bodies under the influence of aerodynamic loads. The study found that the safety factor of the door and window corners of the side wall of the car body is relatively small, and the aerodynamic load has a greater impact on the side wall, and fatigue failure is prone to occur under the action of aerodynamic load. [Gong and Zhu \(2018\)](#) studied the response mechanism of the tunnel lining under the coupling effect of the flow field and the surrounding rock, and concluded that the time course of the displacement decrease when the train passes through the tunnel in a single time fluctuates. In the vertical direction of the lining, the dynamic load response decreases as the depth increases, and the tunnel lining is more likely to be damaged under tensile stress. The above research can well illustrate that the aerodynamic effect in the tunnel cannot be ignored. The literature mostly focuses on the aerodynamic effects inside and on the tunnel wall, and there are few studies on the pressure gradient and load spectrum of the tunnel wall. Because the pressure at the same monitoring point in a tunnel changes constantly, the change time from the peak of the positive pressure to the trough of the negative pressure is very short. Further, sometimes the pressure is small, and the load spectrum and pressure gradient vary greatly, so it is not sufficient to study the peak pressure alone. Under different working conditions, the pressure gradient and frequency spectrum of the tunnel wall should also be analyzed in depth, including the aerodynamic effect of the wall after the train passes through the tunnel.

How to study the aerodynamic effects of tunnel walls under high-speed train operation is very important. To achieve this goal, in recent years, many scholars have conducted extensive research on the aerodynamics of trains passing through tunnels. Some scholars have studied the aerodynamic effects in the tunnel based on numerical simulation. [Wang and Liu \(2013\)](#) studied the aerodynamic pressure of a single train passing through a 70 m^2 single-track tunnel and a 100 m^2 double-track tunnel based on numerical simulation. The pressure at the head and tail of the train varies greatly, and the pressure at the center of the train is basically the same. It also reveals that the wall pressure of the tunnel 20 m before the entrance of the tunnel increases rapidly with the increase of the distance between the measuring point and the tunnel entrance, and the increase becomes slower after 20 m, and reaches the maximum around 200 m. However, the article does not give a detailed explanation of the changing law of aerodynamic pressure on the tunnel wall. [Wei et al. \(2019\)](#) also analyzed the aerodynamic effect when the train passed through a 70 m^2 single-track tunnel at 300 km/h based on numerical simulation, and found that the positive peak, negative peak, and peak-to-peak pressures of the tunnel wall were the largest in the middle of the tunnel, which verified The three-dimensional effect of a single-track tunnel is not obvious. Through three-dimensional numerical simulation, the dynamic process of single-car driving and meeting of trains in the tunnel is calculated, and the superposition relationship

between the pressure wave effect and the pressure wave effect at the entrance of the tunnel is proved. The research has obtained the possible maximum positive and negative gas pressure in the tunnel and its occurrence location; the relationship between gas pressure fluctuations and train speed, and the relationship between the maximum positive pressure value and the maximum negative pressure value and the train speed ([Li and Guan, 2012](#); [Li and Yuan, 2014](#)). [Chen et al. \(2017\)](#) used a three-dimensional compressible turbulence model to simulate the flow and pressure waves of two trains passing each other in the tunnel. The analysis found that the positive peak value of the initial compression wave on the tunnel wall decreased logarithmically with the increase of the length of the nose. During the entire crossover process, the peak-to-peak amplitude of the body surface pressure decreases with the increase of the longitudinal distance from the anterior nose tip. The front of the short train has the greatest influence on the surface pressure, lateral force, overturning moment and the total resistance of the train. [Chu et al. \(2014\)](#) used a three-dimensional compressible model to study the effects of tunnel length, blockage ratio, train speed and crossing position on the interaction of train aerodynamic waves when two trains pass each other in a tunnel. The study found that the train/tunnel interaction, the pressure coefficient and drag coefficient of the train increase with the increase of train speed and blockage ratio. The side force coefficient is affected by the train/train interaction. When two trains are arranged side by side, the side force coefficient reaches the maximum value.

Some scholars have studied the aerodynamic effects in the tunnel based on indoor experiments and field measurements. [Wan and Wu \(2006\)](#) tested the aerodynamic force of the 200 km/h tunnel on the Sui-Yu line and found that in the design of the passenger dedicated line tunnel, it is recommended to consider the aerodynamic effects in the tunnel based on the most unfavorable tunnel length; the comfort criterion for the Chinese high-speed railway tunnel is proposed. [Chen et al. \(2014\)](#) conducted a field test on a high-speed train, and revealed that when the train passes through the tunnel and crosses in the tunnel at speeds of 350 km/h and below, the maximum axle is 41.28 kN horizontally, and the maximum derailment coefficient is 0.70. The heavy load reduction rate is a single peak value of 0.79, the maximum pressure difference between inside and outside the vehicle is 3224 Pa, and the maximum change value of the air pressure inside the vehicle is 1064 Pa for 3 s. [Liu et al. \(2018\)](#) obtained the aerodynamic pressure at different test points in the tunnel based on on-site measurements; analyzed the pressure formation mechanism, amplitude distribution and pressure attenuation. At the same time, it is pointed out that the pressure attenuation coefficient has nothing to do with the train speed, but is related to the length of the tunnel, the test location and the number of tunnel ventilation holes. [Ko et al. \(2012\)](#) conducted a series of on-site measurements near the opening, shaft or tunnel based on the normal operation of the high-speed train in the tunnel. It was found that the compression wave generated at the entrance and exit of the train led to a sharp increase in the pressure in the tunnel; while the entrance and exit of the train produced an expansion wave that caused the pressure to drop. The spatial variation law of the pressure peak induced by the train in the tunnel is discussed, the relationship between the train speed and the pressure peak is established, and the influence of the cross-sectional area of the tunnel on the train speed is given. [Gilbert et al. \(2013\)](#) and [Baker et al. \(2014\)](#) analyzed the influence of the load transient pressure on the railway structure under different conditions (open air, one-sided vertical wall, double vertical walls, partially enclosed spaces, short tunnel and long tunnel) based on the dynamic model test platform. It reveals the changing law of aerodynamic pressure, discusses the relationship between aerodynamic pressure and tunnel length, train length, distance from tunnel entrance, and the law of aerodynamic pressure in different situations. At the same time, the existing European standard formula was revised and evaluated based on the experimental results, and the predicted results are closer to the experimental results.

The literature mostly focuses on the aerodynamic effects inside and

on the tunnel wall, and there are few studies on the pressure gradient and load spectrum of the tunnel wall. Because the pressure at the same monitoring point in a tunnel changes constantly, the change time from the peak of the positive pressure to the trough of the negative pressure is very short. Further, sometimes the pressure is small, and the load spectrum and pressure gradient vary greatly, so it is not sufficient to study the peak pressure alone. Under different working conditions, the pressure gradient and frequency spectrum of the tunnel wall should also be analyzed in depth, including the aerodynamic effect of the wall after the train passes through the tunnel.

This paper uses theoretical analysis, dynamic model tests, and numerical simulation methods to compare the peak pressure, pressure gradient, and aerodynamic load spectrum of a tunnel wall under different working conditions. Commercial software is used to process the results, to provide a basis for studying the fatigue and damage mechanism of a fabricated lining structure under aerodynamic loads in high-speed railway tunnels.

2. Control equations

The Reynolds number in the aerodynamic effect of the high-speed railway tunnel exceeds 10^6 , and it is in a turbulent state. Therefore, the turbulence model and the Navier-Stokes equation must be coupled to solve the problem (Luo et al., 2020; Liu et al., 2020; Zhang et al., 2018). Formulas (1) ~ (3) are Navier-Stokes' continuity equation, momentum conservation equation and energy conservation equation, respectively, and (4) is the gas state equation. Formulas (5) ~ (9) are the theoretical basis for calculation of the RNG K- ϵ turbulence model. All the above equations provide a theoretical basis for the numerical calculation of the aerodynamic effect of high-speed trains entering the tunnel, as follows.

2.1. The continuity equation is

$$\frac{\partial \rho}{\partial t} + \frac{\partial}{\partial x_i} (\rho u_i) = 0, \quad (1)$$

where t, ρ, x_i, u_i represent the time, density, coordinate components, and velocity components, respectively.

The momentum conservation equation, i.e., the compressed N-S equation, is

$$\frac{\partial}{\partial t} (\rho u_i) + \frac{\partial}{\partial x_j} (\rho u_i u_j) = -\frac{\partial P}{\partial x_i} + \frac{\partial}{\partial x_j} \left[\mu \left(\frac{\partial u_i}{\partial x_j} + \frac{\partial u_j}{\partial x_i} - \frac{2}{3} \delta_{ij} \frac{\partial u_k}{\partial x_k} \right) \right], \quad (2)$$

where P is the pressure, μ is the dynamic viscosity coefficient, and δ_{ij} is the second-order unit tensor, where $\delta_{ij} = 1.0$ when $i = j$, and $\delta_{ij} = 0$ when $i \neq j$.

2.2. The energy conservation equation is

$$\frac{\partial}{\partial t} (\rho E) + \frac{\partial}{\partial x_j} [\rho u_j (E + p)] = \frac{\partial}{\partial x_j} \left(K \frac{\partial T}{\partial x_j} + u_i \tau_{ij} \right), \quad (3)$$

where $\tau_{ij} = \mu \left(\frac{\partial u_i}{\partial x_j} + \frac{\partial u_j}{\partial x_i} \right) - \frac{2}{3} \mu \delta_{ij} \frac{\partial u_k}{\partial x_k}$; K is the thermal conductivity; $E = C_v T$, where T is the absolute temperature; E is the total energy per unit volume; and C_v is the specific heat of constant volume.

Assuming that the fluid is a perfectly ideal gas, the equation of state is

$$p = \rho R T, \quad (4)$$

where R is the gas constant.

The above four equations can form a closed equation group, which can be solved numerically.

Based on the Re-Normalization Group (RNG) k - ϵ model, let $\mu_t =$

$\rho C_\mu \frac{k^2}{\epsilon}$ and C_μ be the model constant 0.0845. The transport equations for the increased turbulent flow energy k and the turbulent dissipation rate ϵ are as follows (Wang et al., 2012):

$$\frac{\partial (\rho k)}{\partial t} + \frac{\partial (\rho k u_i)}{\partial x_i} = \frac{\partial}{\partial x_j} \left(\alpha_k u_{eff} \frac{\partial k}{\partial x_j} \right) + G_k + G_b - \rho \epsilon - Y_M + S_k, \quad (5)$$

$$\frac{\partial (\rho \epsilon)}{\partial t} + \frac{\partial (\rho \epsilon u_i)}{\partial x_i} = \frac{\partial}{\partial x_j} \left(\alpha_\epsilon u_{eff} \frac{\partial \epsilon}{\partial x_j} \right) + C_{1\epsilon} \frac{\epsilon}{k} (G_k + C_{3\epsilon} G_b) - C_{2\epsilon} \rho \frac{\epsilon^2}{k} - R_\epsilon + S_\epsilon, \quad (6)$$

where $\alpha_k, \alpha_\epsilon$ is the reciprocal of the effective turbulent Prandtl constant of k, ϵ ,

$$R_\epsilon = \frac{C_\mu \rho \eta^3 (1 - \eta/\eta_0)}{1 + \beta \eta^3} \frac{\epsilon^2}{k}, \quad (7)$$

where $\eta = S_k/\epsilon$, $\eta_0 = 4.38$, $\beta = 0.012$. The turbulence viscosity coefficient satisfies:

$$d \left(\frac{\rho^2 k}{\sqrt{\epsilon \mu}} \right) = 1.72 \frac{\tilde{\nu}}{\sqrt{\tilde{\nu}^3 - 1 - C_v}} d\tilde{\nu}, \quad (8)$$

where $\tilde{\nu} = \mu_{eff}/\mu$ and $C_v \approx 100$.

In addition, the model constants for basic turbulent flow, including air and water obtained from experiments, are:

$$C_{1\epsilon} = 1.42, C_{2\epsilon} = 1.68. \quad (9)$$

3. Numerical model

3.1. Basic assumption

- (1) The tunnel takes a single-hole, double-line section with a cross-sectional area of 100 m². Assuming that the tunnel lines are all straight sections and have no slope, the line spacing is 5 m.
- (2) The study ignores the detailed structures of the upper part of the train, such as the pantograph, bogie, and car body connection. Due to the influence of the surface layer effect on the train surface, the train surface is set as a frictional wall boundary (non-slip boundary), and the train surface roughness is 0.0045 mm. These conditions allow more accurate calculations of the friction resistance and other parameters of the train surface (Xi et al., 2010). Ignoring the detailed structure of the drainage ditch, safety channel, and track in the tunnel, it is assumed that the reinforced concrete wall of the tunnel has a certain roughness, and the equivalent roughness height of the tunnel wall is taken as 5 mm (Li, 2010).
- (3) When trains meet at a constant speed in the tunnel at 400 km/h, the relative speed exceeds Mach 0.6, so the air is calculated as a compressible fluid in the three-dimensional numerical simulation.

3.2. Calculation model

This article adopts the CRH380A high-speed train model, which comes as an 8-car or a 3-car (leading car + middle car + tail car) train. The length, width, and height of the 8-car (3-car) are 201.4 m (77 m), 3.38 m, and 3.7 m, respectively, and the cross-sectional area is 11.2 m². The distance to the bottom of the train is 0.2 m, which is used to simulate the height of the top surface of the rail, as shown in Fig. 1. The unsteady, viscous, compressible N-S equations and RNG two-equation turbulence model are used for simulation. This model has been proven to be effective in the study of aerodynamic effects in high-speed railway tunnels (Liu et al., 2018; Niu et al., 2018b; Tian, 2004).

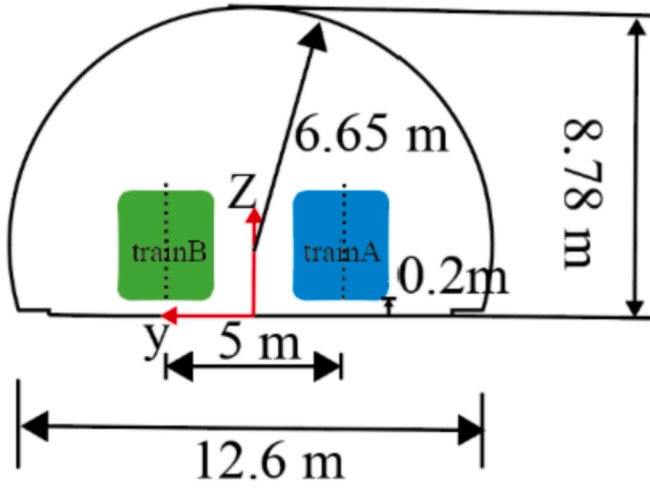


Fig. 1. Schematic diagram of the cross section of a high-speed railway tunnel.

In addition to section 5.3 discussing the aerodynamic pressure on the tunnel wall under different train lengths, the other main discussions are the train length of 8-car and the train speed of 400 km/h. In order to facilitate the comparative analysis of peak pressure and pressure gradient, based on the maximum operating speed of an 8-car CRH380A at 400 km/h and the industry standard (BS EN, 2010, National Railway Administration of the People's Republic of China, 2018), the tunnel length can be calculated as:

$$L_{tu,1} \approx \frac{L_{tr,A}}{4} \cdot \frac{c}{v_{tr,A}} \left(1 + \frac{c}{v_{tr,A}} \right), \quad (10)$$

$$L_{tu,2} \approx \frac{c}{2} \left(\frac{L_{tr,A}}{v_{tr,A}} + \frac{L_{tr,B}}{v_{tr,B}} \right), \quad (11)$$

where $L_{tu,1}$ and $L_{tu,2}$ are the most unfavorable tunnel lengths when a single train passes through the tunnel and when trains meet at the same speed in the tunnel, respectively; $L_{tr,A}$ and $L_{tr,B}$ are the lengths of high-speed trains A and B, respectively; $v_{tr,A}$ and $v_{tr,B}$ are the speeds of high-speed trains A and B, respectively; and c is the empirical coefficient, which approximates the local speed of sound, and its value is 336 m/s.

Therefore, the most unfavorable tunnel lengths when a single train passes through the tunnel and when trains meet at the same speed in the tunnel are 612.7 m and 609.04 m, respectively, and the final tunnel length is 620 m.

3.3. Computational domain and boundary conditions

To ensure that the flow field around the train is fully developed before entering the tunnel, the nose tip of the train head is 100 m from the tunnel entrance. To ensure the full development of the flow field and avoid the influence of boundary conditions on the flow field structure around the train, taking the train's height H as the characteristic length, the calculation domain length \times width \times height on the entrance side and exit side of the tunnel is the same, which is $122H \times 30H \times 16.2H$ (British Standards Institution, 201). Fig. 2 is a schematic diagram of the calculation domain when the train passes through the tunnel. The Cartesian coordinate system is adopted, whose origin is at the tunnel entrance, where the x -, y -, and z -axes represent the respective longitudinal, transverse, and vertical directions of the tunnel. The entire area of the tunnel and the train is discretized with a hexahedral structure grid. The minimum grid size of the train surface and tunnel is 0.006 m and 0.1 m, respectively, as shown in Fig. 3. Among them, Fig. 3(c) shows the geometric models of 8-car and 3-car.

The calculation domain and boundary conditions are shown in Fig. 4. The length of the moving area in Fig. 4 is 4000 m, not only long enough,

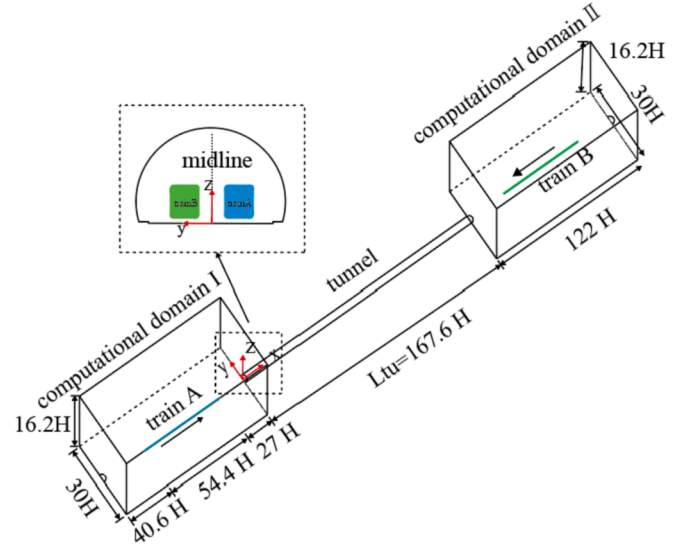


Fig. 2. Schematic diagram of calculation domain when train passes through tunnel.

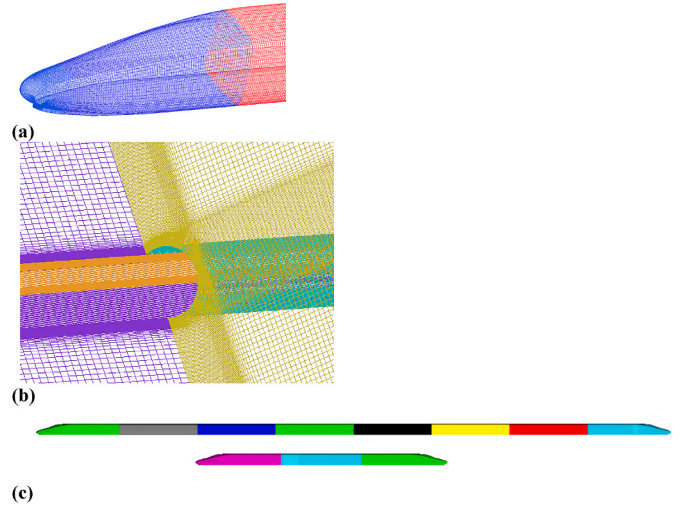


Fig. 3. Grid model of train and tunnel entrance. (a). Train head model. (b). Mesh model at tunnel entrance. (c). 8-car and 3-car models.

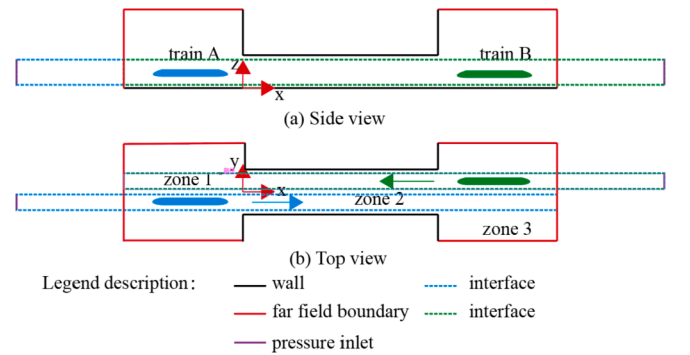


Fig. 4. Schematic diagram of boundary conditions.

but also ensures that the two end faces of the moving area will not enter the static area. The area is divided into three parts, where zones 1 and 2 are sliding areas, and zone 3 is a static area. The boundary conditions are marked in different colors. The red, purple, and black lines represent the

far field, pressure inlet, and wall boundaries, respectively, and the light blue and green lines represent the interface boundary.

3.4. Monitoring point layout

To study the aerodynamic effect and load spectrum of the tunnel wall, 11 monitoring sections were set up in the longitudinal direction, each with two monitoring points. According to Liu et al. (2016), the pressure peak-to-peak value is larger near the middle of the tunnel, so there are relatively more monitoring sections arranged in the middle of the tunnel. At the same time, when the train is just entering the tunnel,

due to the piston effect and friction effect, the pressure changes rapidly, so relatively many measuring points are arranged at the entrance of the tunnel. At other locations, a monitoring section is arranged every 100 m; see Fig. 5(a) for details. Combining with the literature Chu et al. (2014), this paper selects the height of 2.5 m from the track on the tunnel wall to the track for research, as shown in Fig. 5(b). In Fig. 5(a), the two rows represent the left and right lines, respectively, in the tunnel. The measurement points are 25 m, 50 m, 100 m, 200 m, 250 m, 300 m, 310 m, 350 m, 400 m, 500 m, and 600 m from the tunnel entrance. As shown in Fig. 5(b), two monitoring points, A and B, are arranged in the cross section. For clarity, we analyze only some of the monitoring points

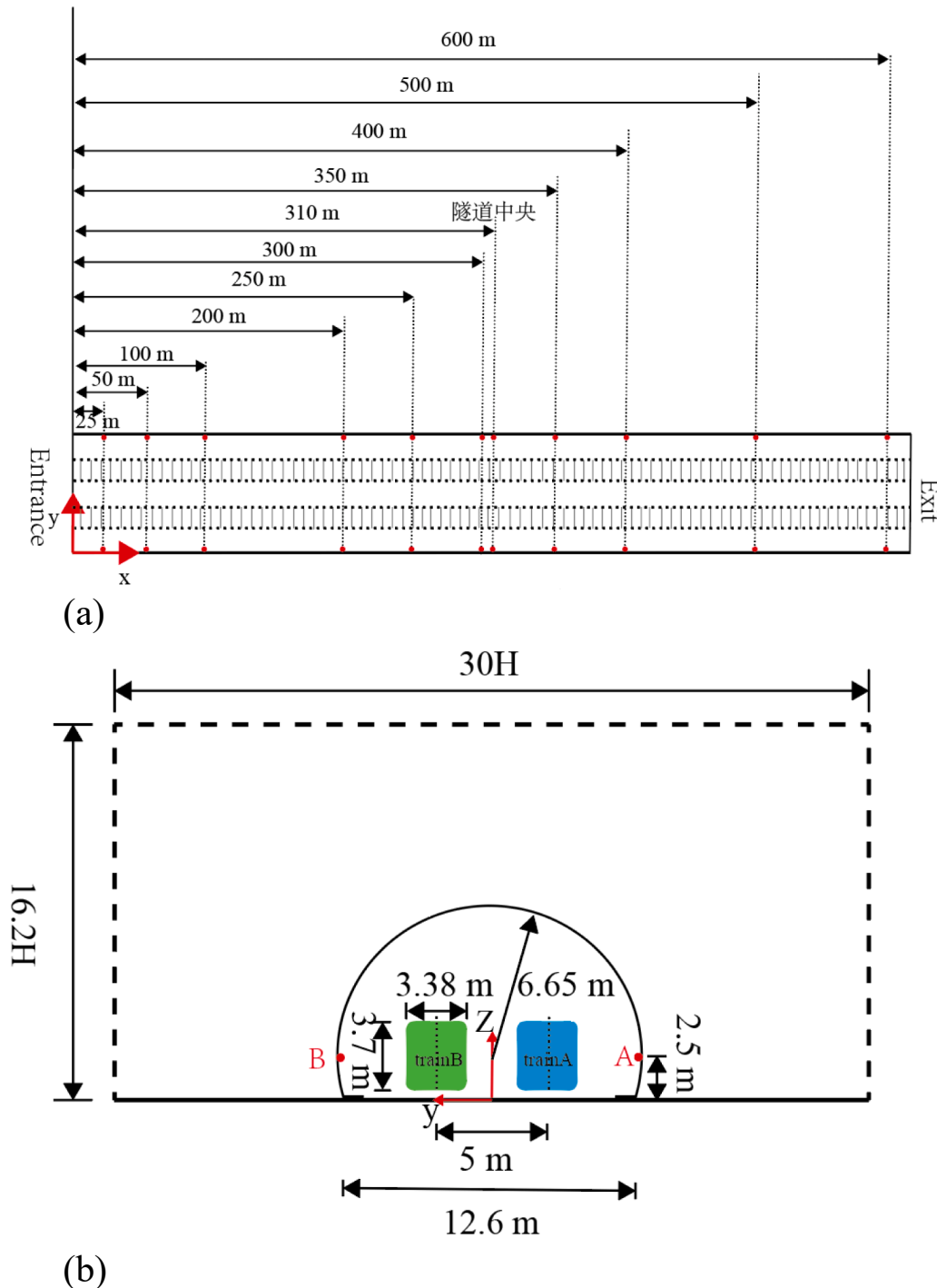


Fig. 5. Arrangement of the monitoring points. (a) Layout drawing of monitoring points in longitudinal section of tunnel. (b) Layout of cross-section monitoring points.

below.

3.5. Numerical calculation method

In this paper, the fluid calculation software Fluent is used to solve the problem, and the control equations are solved discretely by the finite volume method. The fluid pressure and velocity are coupled using the SIMPLE algorithm, and the pressure is corrected by the iterative method. The second-order upwind style is used to discretize the convection and diffusion terms, and the second-order implicit format is used to discretize the time derivative for unsteady flow calculations. The calculation time step is 0.002 s, and the number of iterations for each time step is 50.

To avoid regenerating the grid during calculation, ensure the conservation of flow field flux, and reduce the calculation cost, the sliding mesh is used for numerical calculation (Jiang et al., 2019; Ricco et al., 2007). We simulate the relative movement between the train and tunnel. When area 2 moves forward and area 1 remains stationary, there will be an exchange surface between the stationary and moving areas, and the information of the two flow fields is transmitted through the interface in the middle, thereby solving the flux ϕ entering the two-region unit, which ensures the conservation of flow field flux. In the analysis, the boundary surfaces of areas 1 and 2 are A-B-C and D-E-F, respectively. During the calculation process, the two boundaries slide relative to each other to form an exchange surface a-d-b-e-f. The information of unit 4 is transmitted to unit 1, unit 2, and unit 3 through plane d-b-e. The information of unit 5 is transferred to unit 3 through face e-f. In the end, simulation by sliding grid technology ensures the conservation of the flow field flux. Fig. 6 is a schematic diagram of the sliding mesh technique used to compute the flux across two parts of each grid interface.

In any control volume, when simulating a sliding grid of a moving boundary, the integral conservation equation of a generalized scalar ϕ is

$$\frac{d}{dx} \int_V \rho \phi dV + \int_{\partial V} \rho \phi (u - u_g) dA = \int_{\partial V} \Gamma \nabla \phi \cdot dA + \int_V S_\phi dV, \quad (12)$$

where ∂V is the boundary of the control volume, u_g is the slip velocity of the slip grid, u is the velocity vector, V is the control volume, A is the control area, Γ is the diffusion coefficient, and S_ϕ is the source term.

4. Experimental verification of algorithm

We used 1:8 dynamic model experimental data to verify the correctness and reliability of the numerical method in this paper. The numerical simulation used the unsteady, viscous, compressible N-S equation and the RNG two-equation turbulence model. During the numerical verification, the shape and size of the tunnel in the simulation model are completely consistent with the 1:8 dynamic model test parameters, as shown in Fig. 7(a). In the dynamic model test and the numerical simulation, the train length is 9.9 m, and the train model is the same, and the train speed is the same, both are 304 km/h. This can ensure that the train enters the tunnel to produce the same initial

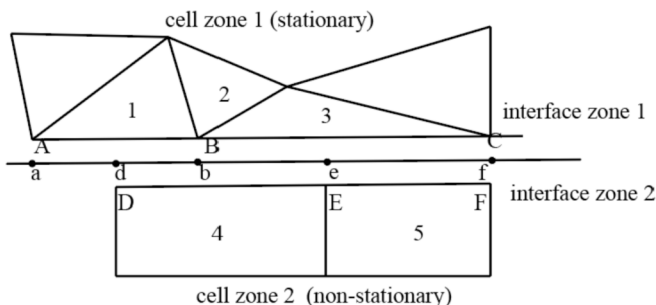


Fig. 6. Schematic diagram of sliding grid method.

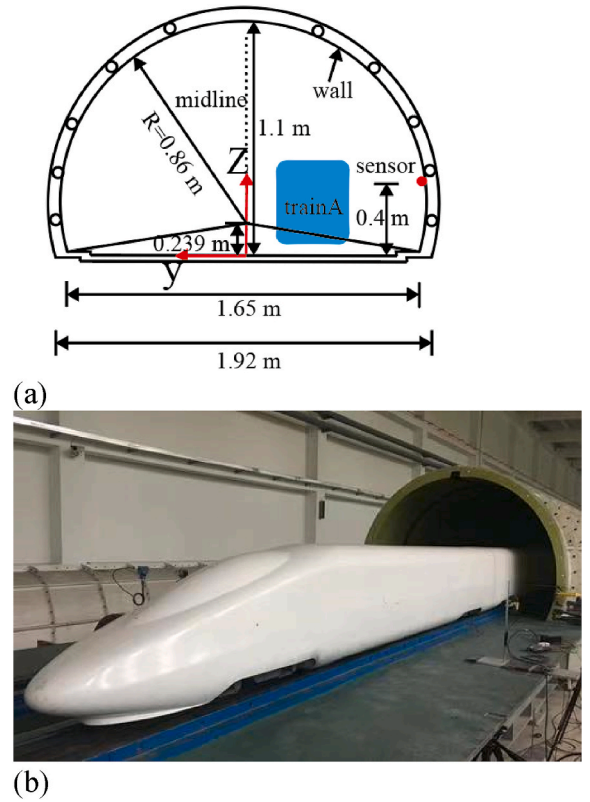


Fig. 7. (a) Sectional dimension of the tunnel model, and (b) mobile model test device.

compression wave. In the numerical simulation, the distance between the starting point of train operation and the tunnel entrance is 25.332 m. The aerodynamic pressure monitoring points were arranged on the tunnel side 20 m and 55 m away from the tunnel entrance, and the measuring points are 0.4 m away from the track surface. The dynamic model test device is shown in Fig. 7(b). The measuring range of the pressure sensor on the tunnel wall was 7000 Pa, the sampling frequency of the data acquisition system was 5 kHz, and the A/D sampling accuracy was 16 bits.

Fig. 8 is a comparison diagram of the dynamic model test data and numerical calculation results of the tunnel wall pressure, and Fig. 8 (a) and (b) are the comparison curves of the wall pressure at a distance of 20 m and 55 m from the tunnel entrance, respectively. There is a certain deviation between the measured data of the dynamic model and the calculated results. This may be due to the difference between the actual measurement reference calibration value and the numerical calculation reference pressure. The main purpose of dynamic model data verification is to compare the pressure values. The main indicators for evaluating the pressure change of the measured and calculated values are the positive peak pressure (P_{max}), negative peak pressure (P_{min}), and pressure peak-to-peak, as shown in Table 1, whose deviations at 20 m from the tunnel entrance are observed to be 0.36%, 0.59%, and 0.22%; the deviations at 55 m from the tunnel entrance are observed to be 8.61%, 0.84%, and 4.04%, respectively, all of which are within the allowable deviation range.

According to Niu et al. (2018a), the numerical simulation of the influence of Reynolds number on the aerodynamic pressure of the tunnel was carried out and it was found that the Reynolds number effect has an influence on the average amplitude of the pressure wave. According to Baker et al. (2019) and Tian (2007), it can be known that the fluid has two self-simulation zones, namely the first and second self-simulation zones. When the model and the prototype are in the second self-simulation zone, the Reynolds numbers of the two do not have to be

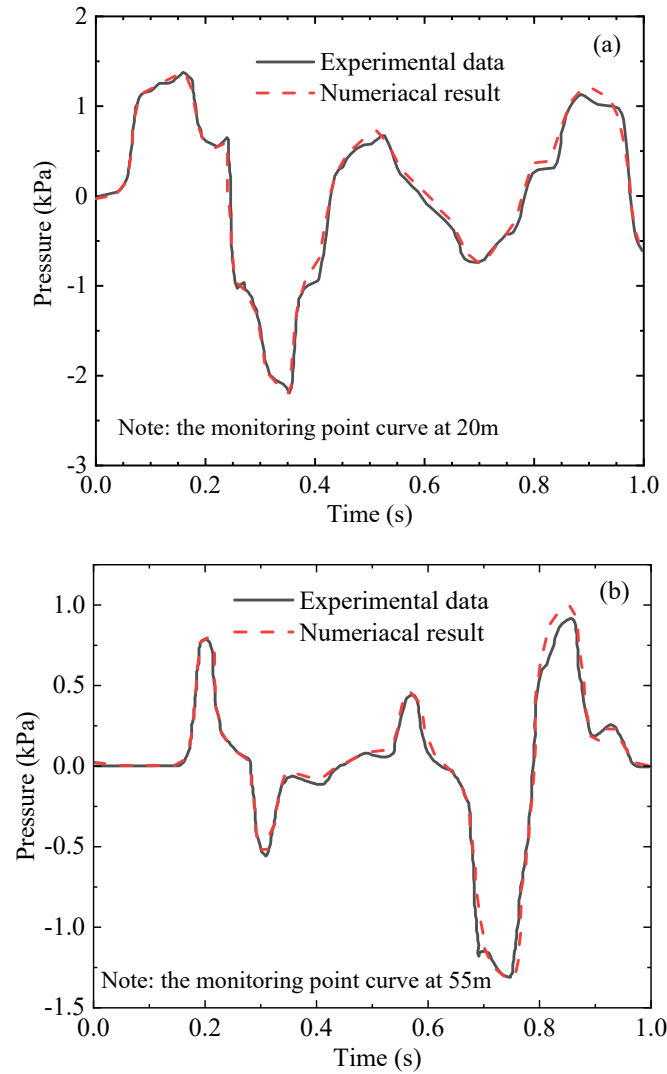


Fig. 8. Comparison of dynamic model test and numerical simulation results.

Table 1

Main indicators for evaluating pressure changes.

Variable		Mobile model test index (kPa)	Numerical calculation index (kPa)	Deviation (%)
Monitoring point at 20 m	P_{max}	1.377	1.372	0.36%
	P_{min}	-2.193	-2.206	0.59%
	peak – to – peak	3.57	3.578	0.22%
Monitoring point at 55 m	P_{max}	0.917	0.996	8.61%
	P_{min}	-1.309	-1.32	0.84%
	peak – to – peak	2.226	2.316	4.04%

equal, and the model test results can be used for the prototype. The first self-mode zone is when Re is less than the first critical value, the flow presents a laminar flow state. The second self-simulation zone refers to the situation where the Reynolds number is very large (close to 10^6) after the flow has fully developed into turbulent flow. For the high-speed train dynamic model test, the model contour length $L = 9.9$ m, the air density $\rho = 1.225$ kg/m³, the dynamic viscosity coefficient of the air $\mu = 1.8 \times 10^{-5}$ kg/m.s, and the test speed is 84.44 m/s (304 km/h), $Re = 5.69 \times 10^7 > 10^6$, the air flow field is in the second self-simulation zone, and the test meets the Reynolds criterion, which can be directly applied to the prototype size.

5. Results and analysis

5.1. Transient pressure analysis

Fig. 9 shows the pressure time-history curve of monitoring point A near the tunnel side at 25 m, 100 m, 300 m, and 600 m from the tunnel entrance when an 8-car enters and exits the tunnel at a speed of 400 km/h from 100 m from the tunnel entrance. Since monitoring point A is near the train, the pressure of monitoring point A is slightly greater than the pressure of monitoring point B when the train passes through the tunnel, only the transient pressure of measuring point A is analyzed. As shown in Fig. 9, as the monitoring point approaches the center of the tunnel, the pressure is greater, and the positive and negative pressure waveforms are square; the monitoring point is close to the tunnel exit. Due to the friction effect of the tunnel wall, the pressure is small, the peak value drops, and the shape tends to be flat. When the train leaves the tunnel, the pressure A at the monitoring point 600 m in the longitudinal direction of the tunnel is 200 Pa higher than the pressure B when the train passes through the tunnel; the aerodynamic pressure on the tunnel wall will continue for a period of time. According to the form of aerodynamic load, it can be determined that when the train passes through the tunnel, the pressure wave on the tunnel wall presents an acyclic state. This is because the pressure changes from squeezing and exhausting air to leaving a vacuum when the train moves. At the same time, the compression wave generated by the train head entering the tunnel (and the expansion wave generated by the tail entering the tunnel) is reflected back and forth at the entrance and exit of the tunnel, which also produces pressure changes. The superposition of the two causes the pressure wave on the tunnel wall to appear non-periodic. When the train completely exits the tunnel, the compression and expansion waves continue to propagate and superimpose in the tunnel, and when they are affected by the friction of the tunnel wall, they continue to decay periodically. Therefore, when analyzing the aerodynamic effect of the tunnel wall, not only the aerodynamic effects of the train passing through the tunnel must be analyzed; the effects of the aerodynamic load on the tunnel wall structure after the train exits the tunnel cannot be ignored.

Fig. 10 shows the pressure time history curve and wave system diagram when the train passes through the tunnel at 400 km/h. The red solid line and light green solid line are the running trajectories of the train head and rear, respectively; the black solid line is the compression wave generated by the train head entering the tunnel, and the black dashed line is the expansion wave formed by the compression wave

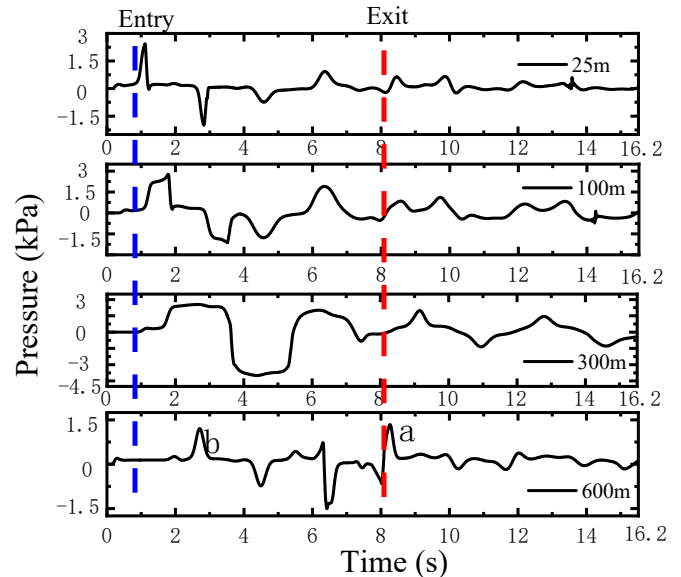


Fig. 9. Pressure time history curves at four different monitoring points.

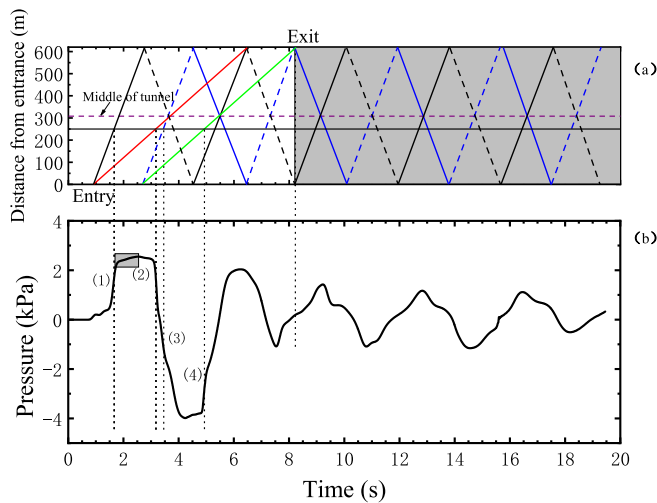


Fig. 10. (a) Wave system at the monitoring point 250 m from the tunnel entrance, and (b) diagram of pressure time history.

generated by the train head reflected at the tunnel exit; the blue dashed line is the expansion wave generated by the train's rear entering the tunnel, and the blue solid line is the compression wave formed by the reflection of the expansion wave from the train's rear at the tunnel exit.

The formation mechanism of the aerodynamic pressure wave when the train passes through the tunnel is shown in Fig. 10. When the compression wave generated by the train head entering the tunnel propagates to the monitoring point, the air pressure rises rapidly, corresponding to (1). As the train continues to enter the tunnel, under the combined action of the tunnel wall and the train, the frictional resistance gradually increases and the aerodynamic pressure rises slowly, corresponding to the small gray mark. When the train passes through the monitoring point, the pressure suddenly decreases because the train induces slipstream to make the airflow speed suddenly increase, and the pressure suddenly decreases, as seen at (2). When the expansion wave of the train's rear reaches the monitoring point, the aerodynamic pressure suddenly drops, corresponding to (3). When the rear of the train passes through the monitoring point, the pressure there suddenly rises, corresponding to (4). After the train exits the tunnel, the pressure time history wave is the result of the back-and-forth transmission and superposition of the entrance compression wave or expansion wave, which corresponds to the large gray mark.

5.2. Aerodynamic effects of train speed

To study the aerodynamic effects of the tunnel wall at different train speeds, we analyze the pressure time history, peak pressure, and pressure gradient changes at monitoring point A in the middle of the tunnel wall when the train passes through the double-track tunnel at three speeds. The peak pressures at different longitudinal monitoring points on the tunnel wall are shown in Fig. 11, and the pressure gradient time history curve of central monitoring point A on the tunnel wall at different speeds is shown in Fig. 12. Table 2 compares the peak pressure and peak pressure gradient of the tunnel wall when the train passes through the tunnel at different speeds.

From the calculation results, it can be seen that from the tunnel entrance to 200 m, the peak-to-peak pressure (maximum positive pressure peak – maximum negative pressure peak) of the tunnel wall is small, but the rate of change is large. Because it is close to the tunnel entrance, the compression and expansion waves at the monitoring point at the tunnel wall have a relatively close action time, and are prone to interfere with each other, resulting in small pressure peaks at the monitoring point. As the train continues to enter the tunnel, the pressure wave is greatly affected by the propagation mode, but less so by the

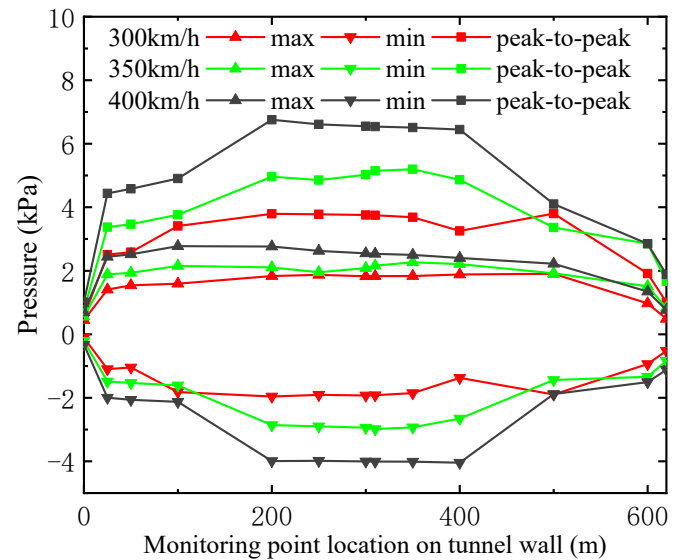


Fig. 11. Pressure peaks at different longitudinal monitoring points on the tunnel wall.

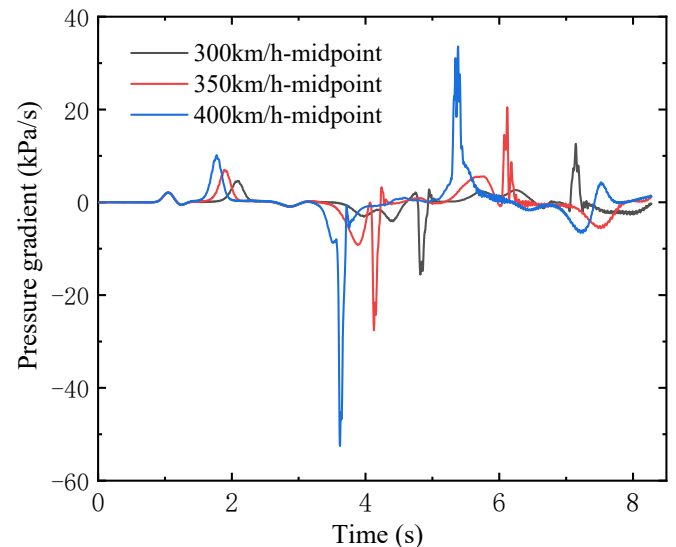


Fig. 12. Time history curve of pressure gradient at monitoring point A on the tunnel wall.

dissipation effect of the external open space, resulting in an increase in the rate of change of the peak pressure from the tunnel entrance to 200 m. However, the maximum pressure peak-to-peak value is mainly concentrated in the range of -110 m to +90 m from the central monitoring point of the tunnel because the central space of the tunnel is more limited than the entrance space. At this time, the compression or expansion wave is concentrated and lasts longer. The waveform can develop fully but does not diverge, which will generate stronger pressure. As the train speed increases, the peak-to-peak pressure gradually increases. The maximum pressure peak-to-peak values when the train passes through the tunnel at 300 km/h and 350 km/h, respectively, are only 26.4% and 36.1% of the maximum pressure peak-to-peak value when the train passes through the tunnel at 400 km/h. Thus, the 400 km/h train speed results in a significant increase in the peak-to-peak pressure.

Because the aerodynamic pressure (including the pressure at the same monitoring point) formed when the train passes through the tunnel changes all the time, it is not enough to study the pressure peak; the

Table 2
Aerodynamic effect parameters of tunnel wall under different train speeds.

Different speeds Pressure and pressure gradient		Train speed (km/h)		
		300	350	400
Tunnel wall pressure when train passes	Peak-peak value (kPa)	3.79	5.20	14.40
	Ratio (%)	26.4	36.1	100
Pressure gradient of tunnel wall when train passes	Peak value of the head (kPa)	1.45	1.95	2.55
	Negative peak value of the head (kPa)	-1.13	-1.85	-2.35
	Pressure gradient of the head - Peak value (kPa/s)	15.59	27.58	52.53
	Ratio (%)	29.7	52.5	100
	Negative peak value of the tail (kPa)	-1.93	-2.96	-4.0
	Peak value of the tail (kPa)	1.22	1.62	2.02
	Pressure gradient of the tail (kPa/s)	4.97	7.37	27.55
	Ratio (%)	18.04	26.75	100

speed of the pressure change, i.e., the pressure gradient, should also be considered. Since the peak-to-peak pressure at central monitoring point A is close to the maximum value, this point on the central wall of the tunnel is used to analyze the pressure gradient peak value at different speeds. From Fig. 12 and Table 2, when the train is monitored by the tunnel wall surface, the speed increase from 300 km/h to 400 km/h, the positive pressure peak increases from 1.45 kPa to 2.55 kPa, and the growth rate is 75.8%; the negative pressure peak increased from 1.93 kPa to 4.0 kPa, and the growth rate was 107.3%. The absolute value of the negative pressure peak is not only greater than the positive pressure peak, but also its growth rate is greater than the positive pressure peak. The positive pressure of the head car is higher than that of the negative pressure is due to the rapid expansion of the compressed air flow caused by the train through the tunnel measuring point, and therefore generates a certain energy loss, so the negative pressure formed is less than the positive pressure impact. The positive pressure of the tail is caused by the airflow impact carried by the train, so the absolute value is minimized in four pressure waves. From Table 2, it can be revealed that as the train speed is gradually increased, the pressure gradient gradually increases. When the train passes through the tunnel at 300 km/h and 350 km/h, the pressure gradient peaks at monitoring point A are only 29.7% and 52.5%, respectively, of the peak pressure gradient when the head of train passes through at 400 km/h. While the train passes through the tunnel at 300 km/h and 350 km/h, the pressure gradient peaks at monitoring point A are only 18.04% and 26.75%, respectively, of the peak pressure gradient when the tail of train passes through at 400 km/h. It can be revealed that the maximum pressure gradient appears between the peak and valley of the head wave, which is due to the growth time of the train head wave longer than the reduction time, and the increase time of the tail wave is shorter than the short time.

5.3. Aerodynamic effects of train length

To explore the aerodynamic effects of the tunnel wall under different train lengths, we analyze the pressure time history, peak pressure, and pressure gradient changes at monitoring point A in the middle of the tunnel when the train passes through at 400 km/h. The pressure time history curve of the central monitoring point on the tunnel wall is shown in Fig. 13, the peak pressure at the longitudinal monitoring point is shown in Fig. 14, and the pressure gradient time history curve of the longitudinal monitoring point is shown in Fig. 15. Table 3 compares the peak-to-peak pressure and pressure gradient peak at the monitoring points when different train lengths pass through the tunnel.

The calculation results show that when trains of different lengths pass through the same tunnel, the pressure time history curves within a section of the entrance are almost the same, because different train

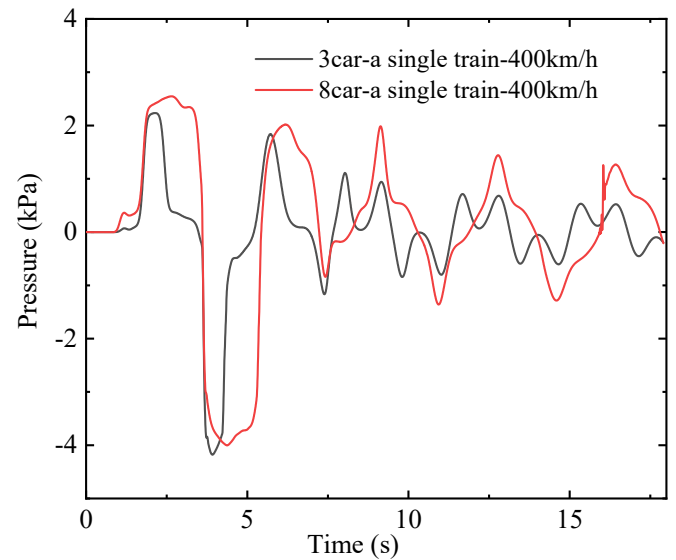


Fig. 13. Time history curve of pressure at monitoring point A in the middle of tunnel wall.

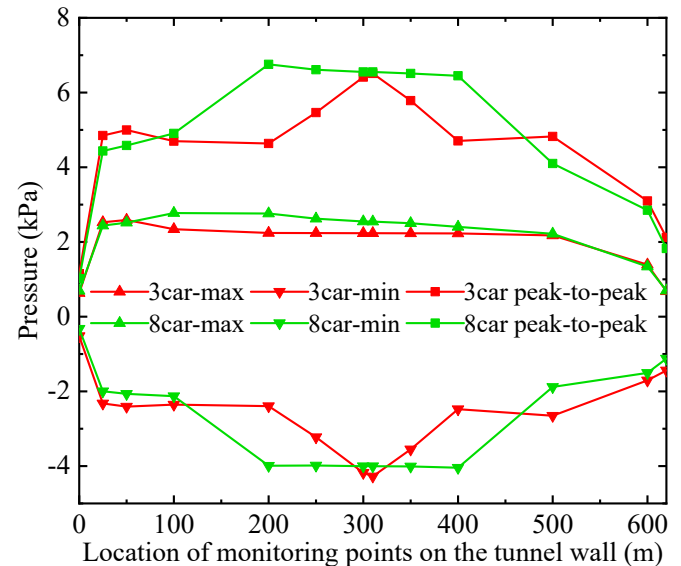


Fig. 14. Peak pressure of different longitudinal monitoring points on the tunnel wall.

lengths run at the same speed and head shape, and therefore cause the same compression wave. The 8-car train can cause greater pressure on the tunnel wall because the longer friction effect makes the pressure rise more. At the same time, the time interval between the head and tail of the 8-car train passing through the tunnel is large, making the time interval of the compression or expansion wave longer, so the pressure rises or falls to a greater extent. The 3-car's tail enters earlier than the 8-car's tail, and it can be seen from Fig. 14 that the peak negative pressure of the 3-car is greater than that of the 8-car within a certain range of the tunnel entrance; these negative pressure peaks are all affected by the expansion wave generated at the rear of the car. As the train moves further into the tunnel, the peak-to-peak pressure of the 3-car reaches the maximum at the central monitoring point, while that of the 8-car is mainly concentrated in the range of -110 m to +90 m at the central monitoring point. Overall, the average pressure peak-to-peak value of the monitoring points near the center of the tunnel is greater for the 8-car than for the 3-car, for the reasons described above.

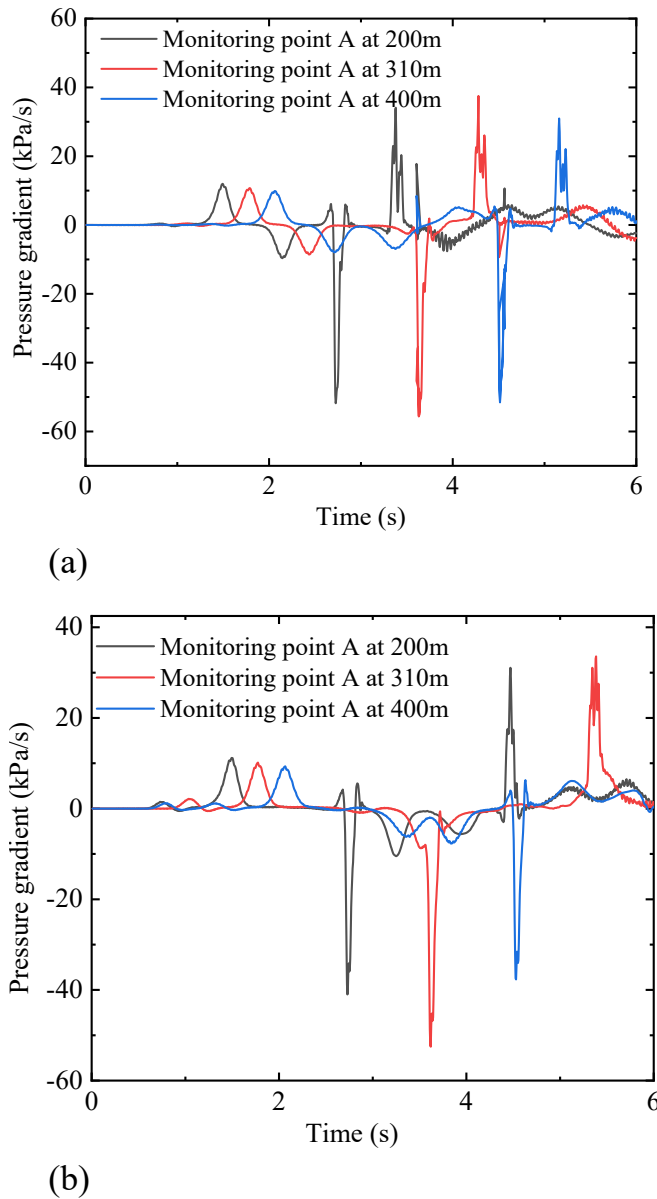


Fig. 15. Time history curve of pressure gradient at different longitudinal monitoring points in tunnel. (a) Pressure gradient time history curve of 3-car-400 km/h. (b) Pressure gradient time history curve of 8-car-400 km/h.

Based on the above analysis, monitoring point A at different longitudinal positions from the entrance of the tunnel is selected for pressure gradient analysis. As shown in Fig. 15, the pressure gradients of the

monitoring points at different longitudinal positions of the tunnel under different train lengths are similar, and the peak pressure gradient of the 3-car is slightly larger than that of the 8-car. This is because the 3-car is relatively short, which causes the change time from the peak moment to the valley moment of the head wave to be shorter than that of the 8-car.

Table 3 selects two different train lengths to analyze the peak pressure and pressure gradient on the wall when the train passes through the tunnel. It can be seen from Table 3 that when different train lengths pass through the same tunnel, the positive peak pressures all appear at the peak of the train's head, and the negative peak pressures all appear at the valley of the train's tail, which is consistent with the rule analyzed in Section 4.2. By analyzing the pressure gradient of the train passing through the tunnel wall, it can be found that the maximum pressure gradient caused by 3 car passing through the center of the tunnel and nearby wall measurement points (200 m, 310 m and 400 m) is relatively close, which is 51.53–55.65 kPa/s, the maximum pressure gradient occurs in the middle of the tunnel. However, the peak pressure gradient caused by 8-car changes greatly. Taking the maximum pressure gradient 52.53 kPa/s caused by the train's head on the central wall of the tunnel as a benchmark, the peak pressure gradients at the measuring points 200 m and 400 m from the tunnel entrance are only 78.1% and 71.73%. The peak pressure gradient produced by the train's head is significantly stronger than the peak pressure gradient produced by the train's tail. The maximum pressure gradient produced by the train's tail is 31.68 kPa/s, which is only 56.9% of the train's head peak pressure gradient. So, such a large peak pressure gradient caused by the train's head will cause fatigue damage to the tunnel structure and temporary facilities under long-term cycling. Therefore, when considering the peak-to-peak pressure of the tunnel wall, the peak pressure gradient cannot be ignored.

5.4. Influence of single train and midpoint intersection on aerodynamic effects

To analyze the influence of aerodynamic effects on the tunnel wall under different train driving modes, we analyze the pressure time history, peak pressure, and pressure gradient changes at central monitoring point A when the 8-car passes through the tunnel at 400 km/h, with a single train or two trains at a constant speed. The pressure time history curve of the central monitoring point is shown in Fig. 16, the peak pressure of the longitudinal monitoring point is shown in Fig. 17, and the pressure gradient time history curve is shown in Fig. 18. Table 4 compares the peak-to-peak pressure of the tunnel wall and the pressure gradient when the 8-car passes through the tunnel in different operating modes.

As shown in Figs. 16 and 17, the pressure changes at the same monitoring point are similar. When two trains pass through the tunnel at the same speed, the pressure at the same monitoring point on the tunnel wall is much stronger than the pressure wave when a single train moves and differs at the central monitoring point on the tunnel wall by a factor of 1.117. This shows that the heads meet at the midpoint of the tunnel,

Table 3
Aerodynamic effect parameters of tunnel wall under different train lengths.

Different train lengths		3-car			8-car		
Monitoring point location (m)		200	310	400	200	310	400
Tunnel wall pressure when train passes	Peak-peak value (kPa)	4.64	6.51	4.71	6.75	6.55	6.45
	Ratio (%)	71.3	100	72.4	103.1	100	98.5
	Peak value of the head (kPa)	2.24	2.23	2.22	2.76	2.55	2.40
	Negative peak value of the head (kPa)	-2.25	-3.96	-2.16	-3.48	-3.52	-3.44
	Pressure gradient of the head - Peak value (kPa/s)	51.83	55.65	51.53	41	52.53	37.68
	Ratio (%)	93.4	100	92.6	78.1	100	71.73
	Negative peak value of the tail (kPa)	-2.4	-4.28	-2.48	-3.99	-4.0	-4.04
	Peak value of the tail (kPa)	1.81	1.84	1.80	2.14	2.06	1.91
	Pressure gradient of the tail (kPa/s)	20.34	31.68	18.66	12.2	27.56	8.85
	Ratio (%)	64.2	100	58.9	44.27	100	32.11

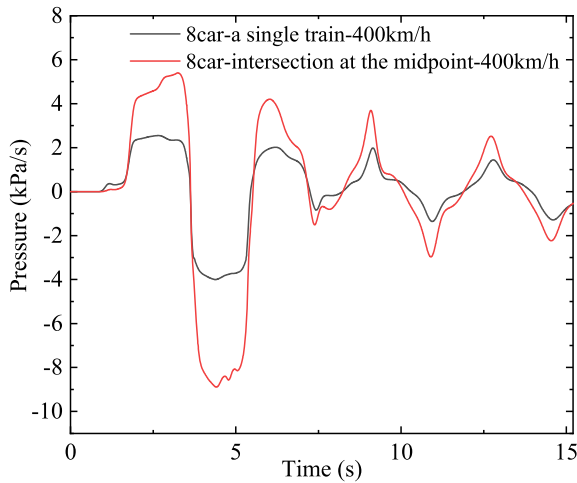


Fig. 16. Pressure time history curve of central monitoring point A on the tunnel wall.

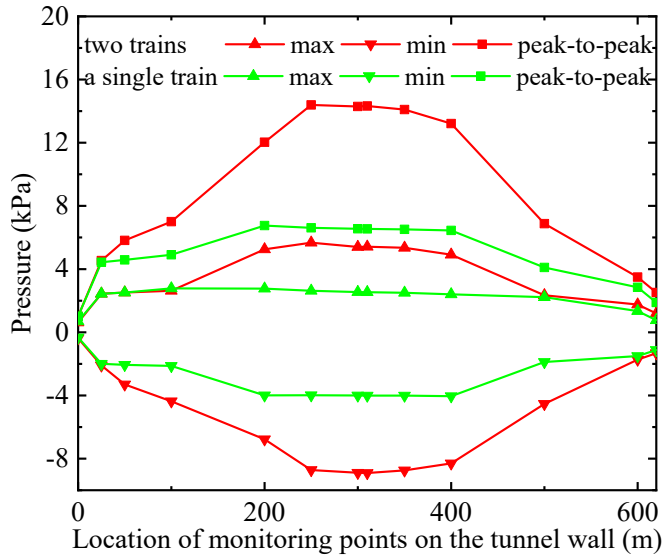


Fig. 17. Peak pressure of longitudinal monitoring point on the tunnel wall.

which causes the interaction of the two pressure fields, generating a large pressure wave in the environment around the midpoint of the tunnel. When two trains intersect at the same speed in the tunnel, the tunnel wall not only bears a higher intensity of aerodynamic pressure, but the pressure wave changes in a short time. Therefore, we must still pay attention to the pressure gradient of the tunnel wall under working conditions. It can be seen from Fig. 18 and Table 4 that when two trains pass through the tunnel at the same speed, the peak pressure gradient at the center of the tunnel wall is 1.534 times that of a single train, and the maximum pressure gradient reaches 80.58 kPa/s; on the whole, the change ratio of the pressure gradient peak in the range of -110 m to 90 m near the center of the tunnel wall is smaller than the pressure peak-to-peak ratio. Therefore, it is necessary to consider the most unfavorable conditions when analyzing the fatigue and damage of the tunnel lining structure by aerodynamic loads.

5.5. Influence of aerodynamic effects after train passage

Based on the above analysis, the pressure gradient peak and pressure peak-to-peak value of the tunnel wall under different train lengths and speeds are smaller than when two trains pass through the tunnel at the

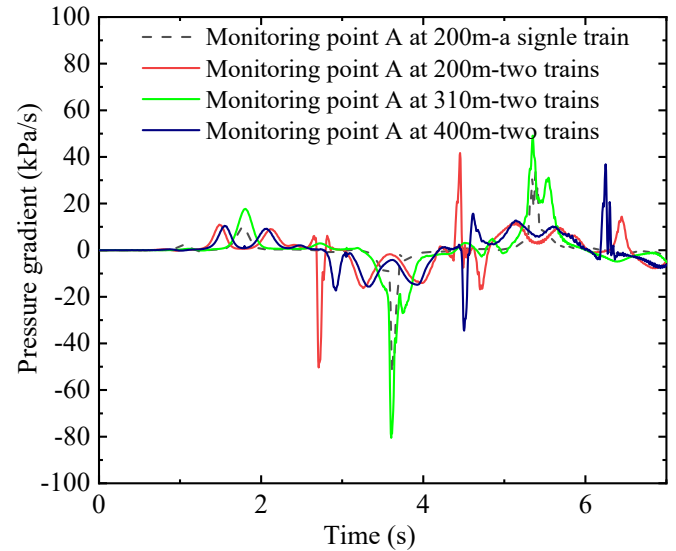


Fig. 18. Time history curve of pressure gradient at different longitudinal monitoring points on the tunnel wall.

Table 4

Aerodynamic effect parameters of tunnel wall under different working conditions.

Situation	Monitoring point location (m)	Tunnel wall pressure when train passes		Pressure gradient of tunnel wall when train passes	
		Peak-peak value (kPa)	Ratio (%)	Peak value (kPa/s)	Ratio (%)
Single train	310	6.75	100%	-52.53	100%
Two trains	200	12.03	178.2%	-50.33	95.8%
	310	14.29	211.7%	-80.58	153.4%
	400	13.2	195.6%	36.84	70.1%

same speed. At the same time, the pressure gradient peak and pressure peak-peak value at the central monitoring point of the tunnel are the largest, and the force at this position is in the most unfavorable state. Combined with the periodic pressure decay of the tunnel wall pressure after the train exits the tunnel, the analysis of the tunnel wall aerodynamic effect after the train passes through the tunnel focuses mainly on central monitoring point A of the tunnel wall under different operating modes. Fig. 19 shows the peak pressure distribution characteristics of central monitoring point A when the 8-car passes through the tunnel at 400 km/h, and Fig. 20 shows the corresponding pressure gradient time history curve.

Two trains intersect at the same speed in the middle of the tunnel. After the train exits the tunnel, the pressure peak and pressure gradient at the monitoring point of the tunnel wall are less than the pressure peak and pressure gradient when two trains pass through the tunnel. But when the two trains intersect at the midpoint, the maximum pressure gradient and pressure peak-to-peak value of the tunnel wall can reach -12.17 kPa/s and 6.66 kPa, respectively. This is only 0.09 kPa less than the peak-to-peak pressure of 6.75 kPa at the central monitoring point of the tunnel wall when a single train passes through the tunnel. Therefore, within 10 min after the train leaves the tunnel, attention should be paid to the aerodynamic pressure on the tunnel wall, especially at the monitoring point in the middle of the tunnel.

5.6. Aerodynamic load analysis

According to relevant research literature (Zhang, 2007; Liu, 2018;

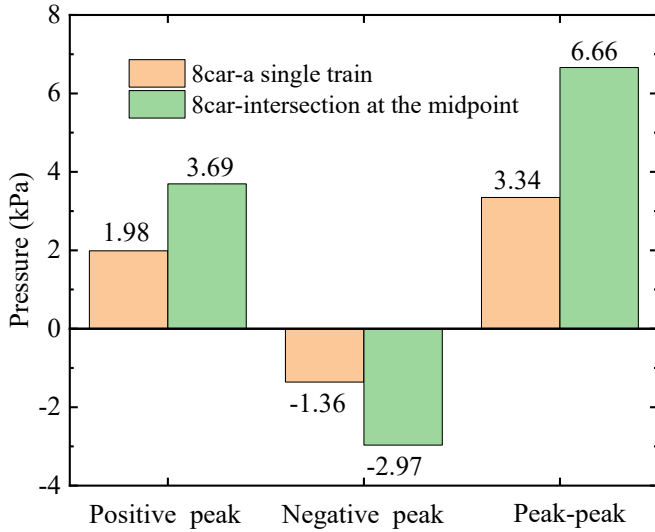


Fig. 19. Distribution characteristics of peak pressure at point A at the center of the tunnel wall.

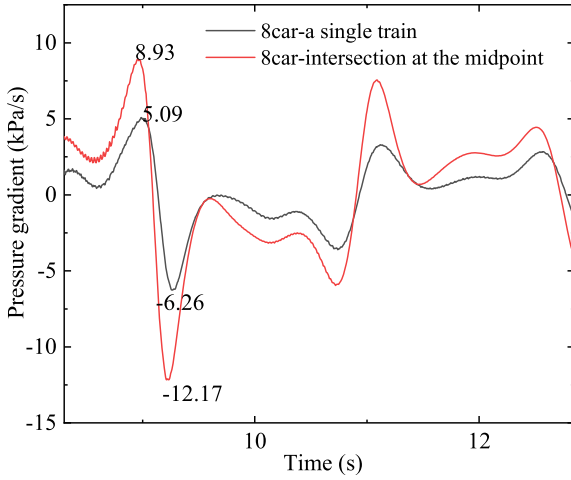
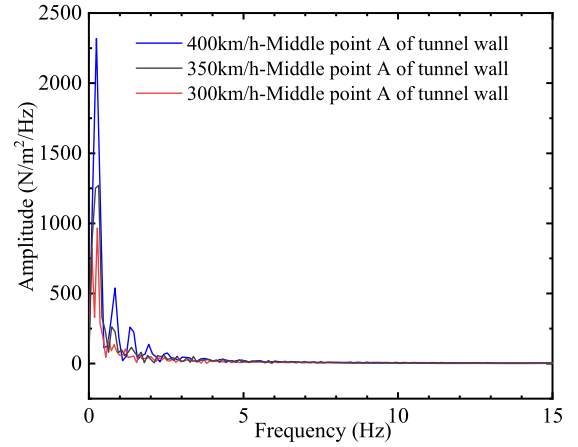


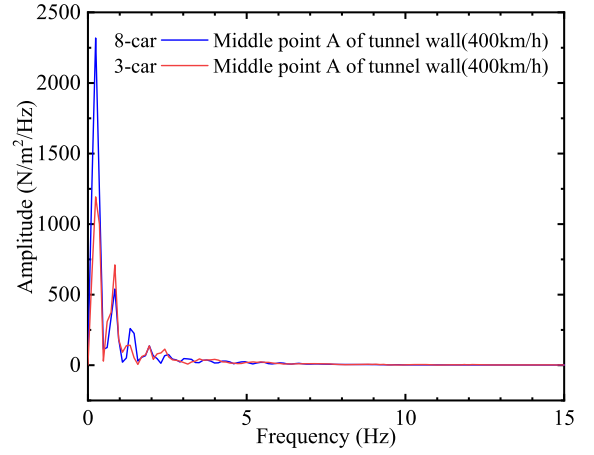
Fig. 20. Time-history curve of pressure gradient at point A at the center of the tunnel wall.

Ying, 1983), the engineering applications of spectrum, power spectrum analysis and random data processing are very extensive, and almost all scientific and engineering departments have applications. Based on the nature of the aerodynamics of high-speed railway tunnels, the study of the fatigue damage of aerodynamic loads to the tunnel lining structure and various facilities in a tunnel should also focus on the aerodynamic load spectra. Based on the pressure time history curve of the tunnel wall obtained by numerical analysis, the pressure spectrum is obtained through a Fourier transform, which can lay the foundation for research of the fatigue damage of the lining structure caused by aerodynamic loads in a high-speed railway tunnel.

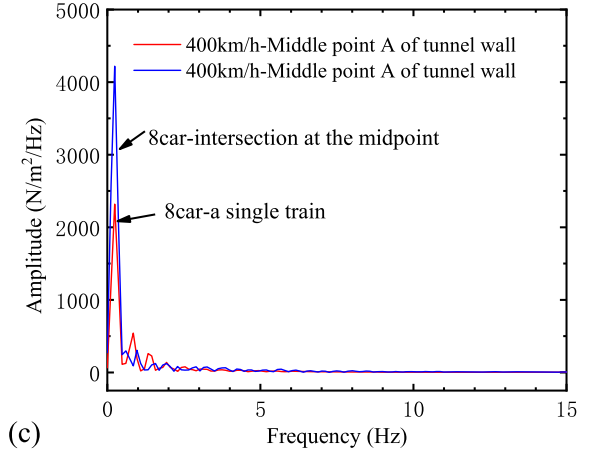
The aerodynamic effect of the tunnel wall when a high-speed train passes through the tunnel is generally higher than after the train passes through the tunnel. Central monitoring point A of the tunnel wall when the train passes through is used for analysis, and the frequency-amplitude curve is obtained through theoretical knowledge, as shown in Fig. 21. Since the time-history curve of tunnel wall pressure when the train passes through is a non-periodic discrete function, $F(t)$, which satisfies the Fourier integral theorem, we apply a Fourier transform to obtain the spectrum function $F(\omega)$ of $F(t)$,



(a)



(b)



(c)

Fig. 21. Frequency amplitude curve of pressure when the vehicle and tunnel are coupled under different working conditions. (a) Frequency-amplitude curve at different train speeds. (b) Frequency-amplitude curve under different train lengths. (c) Frequency-amplitude curve under different train operation modes.

$$F(\omega) = \int_{-\infty}^{\infty} F(t)e^{-j\omega t} dt \text{ or } F(t) = \frac{1}{2\pi} \int_{-\infty}^{\infty} F(\omega)e^{j\omega t} d\omega, \quad (13)$$

where $\omega = 2\pi f$ is the circular frequency, f is the periodic frequency, $j = \sqrt{-1}$, $F(t)$ is the waveform decomposed into a sum of sine functions, and the modulus $|F(\omega)|$ of the spectrum function is the amplitude spectrum of $F(t)$.

Although the pressure-time history curve is non-periodic when the train passes through the tunnel, the Fourier principle shows that any continuously measured time sequence or signal can be expressed as an infinite superposition of sine wave signals of different frequencies. According to this principle, the original signal directly measured is used to perform Fourier transform, and the frequency and amplitude of different sine wave signals in the signal can be obtained in an accumulation manner. At the same time, we can also know from the formula: the projection of $F(t)$ on $e^{j\omega t}$, the integral value is the integral of time from negative infinity to positive infinity, the components of the signal in ω are superimposed at each time, and the result of the superposition is the component of frequency ω , which forms the frequency spectrum. The advantage is that the frequency resolution of the signal is very good, and the frequency components contained in the signal can be clearly obtained, that is, the frequency spectrum. Although the spectrum time is a superposition from negative infinity to positive infinity, when a certain frequency is known, the time location of that frequency cannot be judged. However, for safety reasons, all aerodynamic pressure spectra can be considered as the most unfavorable situation.

When analyzing the aerodynamic characteristics of the train passing through the tunnel, especially the frequency characteristics, it is often difficult to achieve a global quantitative analysis, whether in experiments or numerical calculations. For example, in experiments or numerical calculations, the aerodynamic characteristics are obtained by measuring several local measuring points (such as pressure sensors, or other monitoring means) and performing Fourier analysis. Although it is a quantitative analysis, the calculation results are indeed limited, but it still has a guiding significance for actual engineering. It can better analyze the amplitude characteristics. If the frequency value is coupled with the natural frequency value of the system, it will pose a greater threat to driving safety. It can be seen from Fig. 21 that in the frequency domain, the frequencies with large pressure fluctuations are mainly concentrated in the low frequency range, which are distributed in the range of 0–5 Hz, reflecting the speed of pressure fluctuations. As the frequency increases, the spectral density rapidly decays to 15% of the peak value or even lower. The greater the spectral density, the faster the attenuation. As the train speed increases and the train length increases, the frequency of pressure fluctuations at the measuring point is accelerating, and the magnitude of the pressure fluctuations at the measuring point is also increasing. The peak value of the frequency spectrum of the constant speed two-way train is approximately twice that of the one-way train, and the maximum frequency spectrum can reach 4215 Pa/Hz. The two-way train is more dangerous than other operating conditions.

6. Conclusions

In view of the aerodynamic effects and load spectrum of a high-speed railway tunnel wall, through research and analysis, the following conclusions are drawn.

- (1) When a train passes through a tunnel, the pressure wave on the tunnel wall is in a non-periodic state. When the train completely exits the tunnel, the compression and expansion waves continue to propagate and superimpose in the tunnel, they are affected by the friction of the tunnel wall, and the compression wave and expansion wave continue to decay periodically. At the same measurement point on the tunnel wall, the maximum peak-to-peak pressure on the tunnel wall may occur when the train passes through, or after the train leaves the tunnel.
- (2) When the train passes through the tunnel at 400 km/h, the peak-to-peak pressure of the tunnel wall and the peak pressure gradient increase significantly, and the maximum peak-to-peak pressure is mainly concentrated in the range of -110 m to $+90$ m at the central monitoring point of the tunnel; the pressure gradient appears in the time between the peak and trough moments of the head wave.
- (3) The pressure peak of the monitoring point at the center of the tunnel wall when an 8-car passes through the tunnel is greater than that of a 3-car. This is due to the longer interval between the compression wave and the expansion wave generated by the 8-car, resulting in a larger cumulative impact, and the longer duration of the induced friction effect when the 8-car enters the tunnel. When an 8-car passes through the tunnel, the peak-to-peak pressure of the tunnel wall is at a distance of 200 m from the tunnel entrance, and the peak pressure gradient appears at the central measuring point of the tunnel. Therefore, when analyzing the peak-to-peak pressure of the tunnel wall, the pressure gradient cannot be ignored.
- (4) When two trains meet in the middle of the tunnel, the aerodynamic effect of the tunnel wall is significant. The peak-to-peak pressure of monitoring point A in the middle of the tunnel is about 2.12 times that of a single train; the peak pressure gradient is 1.534 times that of a single train, with a maximum value of 80.58 kPa/s, which is important when studying the damage mechanism of aerodynamic loads on the tunnel lining.
- (5) When the two trains meet at the central monitoring point of the tunnel and exit the tunnel at a constant speed of 400 km/h, the peak-to-peak pressure of the monitoring point in the middle of the tunnel wall is only 0.09 kPa less than when a single train passes through the tunnel. Therefore, within a period of time after the train passes through the tunnel, attention should still be paid to the influence of aerodynamic pressure in the tunnel on the damage of the tunnel lining structure.
- (6) The spectral density is mainly concentrated in the range of 0–5 Hz under different working conditions. The influence of different tunnel lengths on the frequency of aerodynamic loads in the tunnel needs to be further studied.

Funding

This work was funded by the National Natural Science Foundation of China [51878038, 51678036].

Role of the funding source

The funder had no role in experimental design, model establishment, data analysis, manuscript writing, or decisions to submit articles for publication.

CRediT authorship contribution statement

Feilong Li: Conceptualization, Methodology, Investigation, model building, Formal analysis, Writing – original draft. **Jianjun Luo:** Conceptualization, Methodology, Supervision. **Lei Wang:** Verification, Visualization, data management. **Dilong Guo:** Model test guidance, verification, Formal analysis. **Liping Gao:** Writing-commenting and editing.

Declaration of competing interest

The authors declare that they have no known competing financial interests or personal relationships that could have appeared to influence the work reported in this paper.

Acknowledgments

We thank LetPub (www.letpub.com) for its linguistic assistance and scientific consultation during the preparation of this manuscript.

References

- Baker, C., Johnson, T., Flynn, D., Hemida, H., Quinn, A., Soper, D., Sterling, M., 2019. *Train Aerodynamics: Fundamentals and Applications*. Butterworth-Heinemann.
- Baker, C., Jordan, S., Gilbert, T., Quinn, A., Sterling, M., Johnson, T., Lane, J., 2014. Transient aerodynamic pressures and forces on trackside and overhead structures due to passing trains. Part 1: model-scale experiments; Part 2: standards applications. *Proc. Inst. Mech. Eng. - Part F J. Rail Rapid Transit* 228 (1), 37–70. <https://doi.org/10.1177/0954409712464859>.
- Chen, H., Zhang, Y., He, D., Huang, C., 2014. Experimental study on the basic laws of the aerodynamic effect of 350 km/h high speed railway tunnel. *China Railw. Sci.* 35 (1), 55–59. <https://doi.org/10.3969/j.issn.1001-4632.2014.01.09>.
- BS EN 14067-5, 2010. *Railway Applications—Aerodynamics—Part 5. Requirements and Test Procedures for Aerodynamics in Tunnels*.
- Chen, X.D., Liu, T.H., Zhou, X.S., Li, W.H., Xie, T.Z., Chen, Z.W., 2017. Analysis of the aerodynamic effects of different nose lengths on two trains intersecting in a tunnel at 350 km/h. *Tunn. Undergr. Space Technol.* 66, 77–90. <https://doi.org/10.1016/j.tust.2017.04.004>.
- Chu, C.R., Chien, S.Y., Wang, C.Y., Wu, T.R., 2014. Numerical simulation of two trains intersecting in a tunnel. *Tunn. Undergr. Space Technol.* 42, 161–174. <https://doi.org/10.1016/j.tust.2014.02.013>.
- Gilbert, T., Baker, C., Quinn, A., 2013. Aerodynamic pressures around high-speed trains: the transition from unconfined to enclosed spaces. *Proc. Inst. Mech. Eng. - Part F J. Rail Rapid Transit* 227 (6), 609–622. <https://doi.org/10.1177/0954409713494947>.
- Gong, C., Zhu, Z., 2018. Numerical study for the aerodynamic effects of high-speed trains on secondary lining. *Henan Sci.* 36 (5), 721–727. <https://doi.org/10.3969/j.issn.1004-3918.2018.05.017>.
- Ji, W., 2017. Influence of aerodynamic load on secondary lining of high speed railway tunnel with cavity behind vault lining. *China Railw. Sci.* 38 (6), 56–62. <https://doi.org/10.3969/j.issn.1001-4632.2017.06.08>.
- Jiang, Z., Liu, T., Chen, X., Li, W., Guo, Z., Niu, J., 2019. Numerical prediction of the slipstream caused by the trains with different marshalling forms entering a tunnel. *J. Wind Eng. Ind. Aerod.* 189, 276–288. <https://doi.org/10.1016/j.jweia.2019.04.002>.
- Ko, Y.Y., Chen, C.H., Hoe, I.T., Wang, S.T., 2012. Field measurements of aerodynamic pressures in tunnels induced by high speed trains. *J. Wind Eng. Ind. Aerod.* 100 (1), 19–29. <https://doi.org/10.1016/j.jweia.2011.10.008>.
- Li, R., Guan, Y., 2012. Investigation of air pressure pulse when two high-speed trains passing by each other in tunnel. *J. Mech. Eng.* 48 (20), 127–134. <https://doi.org/10.3901/JME.2012.20.127>.
- Li, R., Yuan, L., 2014. Pressure waves in tunnels when high-speed train passing through. *J. Mech. Eng.* 50 (24), 115–121. <https://doi.org/10.3901/JME.2014.24.115>.
- Li, Y., 2010. *Analysis and Theoretical Research on Piston Wind Characteristics of Railway Tunnel Trains*. Lanzhou Jiaotong University, Lanzhou.
- Liu, F., Yao, S., Liu, T.H., Zhang, J., 2016. Real vehicle test analysis of aerodynamic pressure on the wall of high-speed railway tunnel. *J. Zhejiang Univ. Eng. Sci.* 50 (10), 2018–2024. <https://doi.org/10.3785/j.issn.1008-973X.2016.10.024>.
- Liu, F., Yao, S., Zhang, J., Wang, Y.Q., 2018. Field measurements of aerodynamic pressures in high-speed railway tunnels. *Tunn. Undergr. Space Technol.* 72, 97–106. <https://doi.org/10.1016/j.tust.2017.11.018>.
- Liu, R.D., 2018. *Research on Wind-Induced Aerodynamic Characteristics of High-Speed Railway Cavity Wind Barriers*. Beijing Jiaotong University, Beijing.
- Liu, W., Guo, D.L., Zhang, Z.J., Yang, G.W., 2020. Research on dynamic characteristics of high-speed train wake based on POD decomposition. *J. China Railw. Soc.* 42 (9), 49–57. <https://doi.org/10.3969/j.issn.1001-8360.2020.09.007>.
- Lu, Y.H., Feng, Z., Chen, T.L., Zeng, J., Wu, P.B., Pan, J., 2014. Evaluation method of fatigue strength for carbody of high-speed train under influence of aerodynamic loads. *J. Traffic Transport. Eng.* 14 (6), 44–50. <https://doi.org/10.3969/j.issn.1671-1637.2014.06.006>.
- Luo, J., Li, Z., Wang, L., Zhang, D., Wu, Y., 2020. Aerodynamic effect of cross passages at the entrance section of a high-speed railway tunnel in a region with mountains and canyons. *J. Wind Eng. Ind. Aerod.* 204, 104268. <https://doi.org/10.1016/j.jweia.2020.104268>.
- Ma, Y.D., Li, B., Fan, B., 2011. Mesomechanics numerical simulation of high-speed railway tunnel under the action of aerodynamic effect. *J. Dalian Jiaot. Univ.* 32 (4), 16–19. <https://doi.org/10.3969/j.issn.1673-9590.2011.04.004>.
- National Railway Administration of the People's Republic of China, 2018. *Railway Applications-Aerodynamics-Part 3: Requirements and Test Procedures for Aerodynamics in Tunnels*, TB/T 3503.3-2018. China Railway Publishing House, Beijing.
- Niu, J.Q., Zhou, D., Liang, X.F., Liu, S., Liu, T.H., 2018a. Numerical simulation of the Reynolds number effect on the aerodynamic pressure in tunnels. *J. Wind Eng. Ind. Aerod.* 173, 187–198. <https://doi.org/10.1016/j.jweia.2017.12.013>.
- Niu, J., Zhou, D., Liu, F., Yuan, Y., 2018b. Effect of train length on fluctuating aerodynamic pressure wave in tunnels and method for determining the amplitude of pressure wave on trains. *Tunn. Undergr. Space Technol.* 80, 277–289. <https://doi.org/10.1016/j.tust.2018.07.031>.
- Ricco, P., Baron, A., Molteni, P., 2007. Nature of pressure waves induced by a high-speed train travelling through a tunnel. *J. Wind Eng. Ind. Aerod.* 95 (8), 781–808. <https://doi.org/10.1016/j.jweia.2007.01.008>.
- Tian, H.Q., 2004. Research and applications of air pressure pulse from trains passing each other. *J. Railw. Sci. Eng.* 1 (1), 83–89. <https://doi.org/10.3969/j.issn.1672-7029.2004.01.015>.
- Tian, H.Q., 2007. *Train Aerodynamics*. China Railway Publishing House, Beijing.
- Tian, S., Gong, J., 2020. Statistics of railway tunnels in China as of end of 2019. *Tunn. Constr.* 40 (2), 292–297.
- Wan, X., Wu, J., 2006. In-situ test and study on the aerodynamic effect of the rolling stock passing through tunnels with a speed of 200 km/h. *Mod. Tunn. Tech.* 43 (1), 43–48. <https://doi.org/10.3969/j.issn.1009-6582.2006.01.008>.
- Wang, X.Z., Liu, T.H., 2013. Analysis on aerodynamic effects of 350 km/h EMU passing tunnels. *J. Railw. Sci. Eng.* 10 (1), 92–97. <https://doi.org/10.3969/j.issn.1672-7029.2013.01.018>.
- Wang, Y., Yang, G., Huang, C., Wang, W., 2012. Influence of tunnel length on the pressure wave generated by high-speed trains passing each other. *Sci. China Technol. Sci.* 55 (1), 255–263. <https://doi.org/10.1007/s11431-011-4588-5>.
- Wei, Y., Liu, F., Zhang, C., Yang, M., 2019. Numerical simulation and analysis on aerodynamic effects of high-speed train passing through tunnels with 400 km/h. *China Sciencepap* 14 (6), 652–656. <https://doi.org/10.3969/j.issn.2095-2783.2019.06.013>.
- Xi, Y., Mao, J., Li, M., Zhang, N., Ma, X., 2010. Numerical study on the crosswind effects of high-speed train. *J. Beijing Jiaot. Univ.* 34 (1), 14–19. <https://doi.org/10.3969/j.issn.1673-0291.2010.01.004>.
- Yang, Y., Cui, J., 2020. Analysis into the characteristic damaged marks resulted from aerodynamic impact in high-speed-railway tunnel. *Forensic Sci. Technol.* 45 (2), 215–217. <https://doi.org/10.16467/j.1008-3650.2020.02.022>.
- Ying, H.Q., 1983. *Waveform and Spectrum Analysis and Random Data Processing*. China Railway Publishing House, Beijing.
- Zhang, L., Thurow, K., Stoll, N., Liu, H., 2018. Influence of the geometry of equal-transect oblique tunnel portal on compression wave and micro-pressure wave generated by high-speed trains entering tunnels. *J. Wind Eng. Ind. Aerod.* 178, 1–17. <https://doi.org/10.1016/j.jweia.2018.05.003>.
- Zhang, X.Y., 2007. *Research on Aerodynamic Loads in High-Speed Railway Tunnels*. Southwest Jiaotong University, Chengdu.
- Zhao, Y., Ma, W., Cheng, A., Zhang, Q., 2012. *Aerodynamic Effects of High-Speed Railway Tunnels*. China Railway Publishing House, Beijing.